RSC Advances

Graphical Abstract

Covalently Anchored 2, 4, 6-triallyloxy-1, 3, 5-triazine Pd(II) Complex over Modified Surface of SBA-15: Catalytic Application in Hydrogenation Reaction

SBA-15-TAT-Pd(II)

RSC Advances
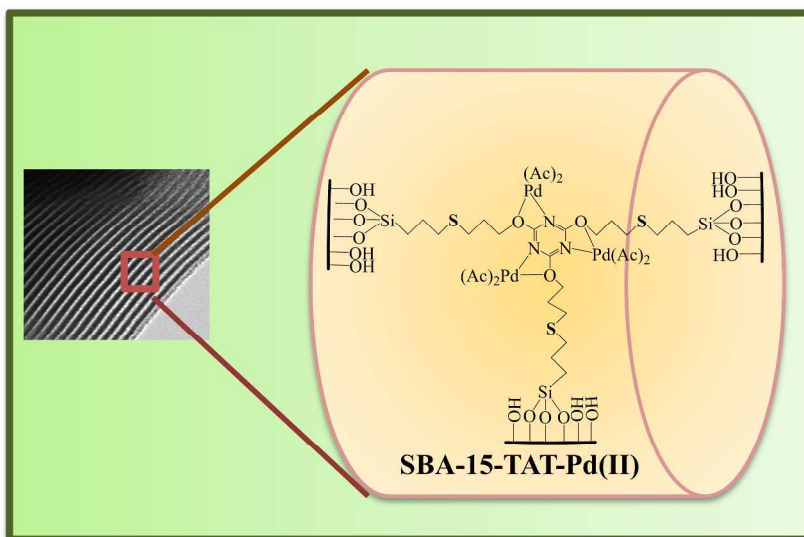
ARTICLE

Covalently Anchored 2, 4, 6-triallyloxy-1, 3, 5-triazine Pd(II) Complex over Modified Surface of SBA-15 : Catalytic Application in Hydrogenation Reaction

Priti Sharma, A. P. Singh*

Highly efficient and reusable SBA-15-TAT-Pd(II) has been synthesized by anchoring 2, 4, 6-triallyloxy-1, 3, 5-triazine (TAT) complex over the organo-functionalized surface of SBA-15. The physiochemical properties of the organo-functionalized catalyst were analyzed by elemental analysis, ICP-OES, XRD, N_2 sorption measurement isotherm, TGA & DTA, solid state ^{13}C, ^{29}Si NMR spectra, FT-IR, XPS, DRS UV-Visible, SEM and TEM. XRD & N_2 sorption analyze to find out textural properties of synthesized catalyst and confirm that ordered mesoporous channel structure was retained even after the multistep synthetic procedures. The electronic environment and oxidation state of Pd in SBA-15-TAT-Pd(II) were monitored by XPS and DRS UV-visible techniques. The catalytic activity of synthesized catalyst SBA-15-TAT-Pd(II) was screened for Hydrogenation reactions and shows higher catalytic activity with good turnover numbers (TON) under optimized experimental conditions with the maxima conversion (>99 %) and selectivity (100 %). The anchored solid catalyst can be recycled efficiently and reused upto five times without major loss in reactivity.

INTRODUCTION

Liquid-phase hydrogenation of olefins using heterogeneous catalysts is an industrially relevant process.[1-3] Along with olefin, hydrogenation of nitro compounds to amines has become one of the most important chemical reactions since organic amines are essential materials for the production of agrochemicals, dyes, pharmaceuticals, polymers and rubbers.[4,5] For more than 100 years chemists have used heterogeneous catalysts based on noble metals on various supports.[6,7] Homogeneous hydrogenation catalysis was developed in the 1960's and is reviewed frequently.[8] It is well known that Pd-catalyzed reactions are of significant importance in modern chemical transformations.[9-11] There is a growing demand for organo-metallic reagents that exhibit favorable chemoselectivity and stereoselectivity in hydrogenation reactions. Generally reaction proceeds using N-ligand based palladium catalysts. However, most of these ligands are expensive and significantly limited to their industrial applications.[12-14] Also some of these new ligands are not easily available and contain tedious and expensive synthesis processes and hardly stable in catalytic systems. Therefore, simple easily accessible stable catalyst is desired for heterogeneous reactions. Unfortunately, the efficient separation and subsequent recycling of homogeneous Pd catalysts remain a scientific challenge. Therefore, developing a facile and expedient approach to separate and recycle catalysts is highly desirable.

Since the discovery of ordered mesoporous silicas,[15] these materials have attracted wide spread attention in both academics and industry due to their huge potential applications.[16,17] Today mesoporous materials have been employed successfully in gas adsorption and storage,[18] sensing,[19] catalysis,[20] optical device[21] and ion exchange.[22] Since the synthesis of ordered mesoporous materials in 1992 sparked worldwide interest in the field of heterogeneous catalysis and separation science; SBA-15 has become the most popular member of the group and possessed extremely high surface area, easily accessible, uniform pore sizes and stability.[23-25] SBA-15 can carry suitable functional groups at their surface, which can effectively interact with relevant metal ion/molecules, which makes them a potential candidate for heterogeneous catalysts. Furthermore, the leaching of the active site can also be avoided as the organic moieties are covalently attached to the inorganic support. Various homogenous complexes were widely used for this transformation via covalent attachment.[26-28]

Accordingly, in the present chapter we report our attempt to graft Pd metal complex of 2, 4, 6-triallyloxy-1, 3, 5-triazine (TAT), derivatives over SBA-15 phases and their catalytic properties in hydrogenation reactions. The immediate goals of our study were (i) to evaluate the heterogenization method of the 2, 4, 6-triallyloxy-1, 3, 5-triazine Pd(II) complex over organic modified SBA-15 support, (ii) to characterize the heterogenized SBA-15-TAT-Pd(II) complexes by various physiochemical techniques (iii) to measure the catalytic properties in hydrogenation reaction and (iv) to determine the extent stability of the catalyst as well as their recycling properties.

The uniqueness of mesoporous structure, phase purity, degree of orderdness and unit cell parameters of all mesoporous materials were determined by powder X-ray diffraction (XRD). XRD pattern of as-synthesized SBA-15, calcined SBA-15, SBA-15-SH, SBA-15-TAT and heterogenized SBA-15-TAT-Pd(II) complexes are visualized in Figure 1. The small-angle XRD pattern in all synthesized samples shows three well-resolved peaks; indexable as (100), (110), (200) reflections associated with *p6mm* hexagonal symmetry. After calcination, the peak intensity of (100) plane increases compared to as-synthesized SBA-15 due to the removal of surfactant molecules. (Figure 1.a, b). It is evident from Figure 1 that XRD patterns of the modified SBA-15 materials are almost similar to the parent SBA-15 with small decrease in overall intensity of (100), (110) and (200) reflections as the organic moieties (-TAT & -SH) get anchored one by one over the mesoporous SBA-15 wall. After organic group modification over SBA-15 by post grafting method, the XRD pattern (Figure 1.b-e) shows that the *p6mm* morphology is preserved.[29] This perseverance of peak positions indicates that partial filling of 2, 4, 6 - triallyloxy-1, 3, 5-triazine Pd(II) complex inside the mesopores is less detrimental to the quality of the SBA-15. The persistence of the (100), (110) and (200) reflections (Figure 1.b-e) not only proved the structural stability of the support but also the existence of long range order even after a number of treatments with organic molecules in solvents. All these observations clearly show that the ordered mesoporosity and structural stability retained even after incorporation of 2, 4, 6-triallyloxy-1, 3, 5-triazine Pd(II) complexes.

The presence of isolated surface silanols, hydrogen bonded hydroxyl group and anchored complex, 2, 4, 6 - triallyloxy-1, 3, 5-triazine Pd(II) are evident from the IR spectrum of calcined SBA-15, SBA-15-SH, SBA-15-TAT and SBA-15-TAT-Pd(II) in Figure 2. The bands observed in the range of 850–770 cm^{-1} account for the symmetric stretching vibrations of the Si-O-Si bonds, while the band at 1090 cm^{-1} is assigned to the asymmetric (Si–O–Si) vibrations.[30] In the hydroxyl region (3200–3600 cm^{-1})[31], a broad, typical peak of Si–O–H and S–H of thiol functionalized SBA-15 were observed at around 3436 cm^{-1} and 468 cm^{-1}, respectively. Propyl thiol-functionalized SBA-15 shows a characteristic peak at 2934 cm^{-1} corresponds to C–H stretching vibrations. The weak bands at 1340 cm^{-1}, 1381 cm^{-1}, 1468 cm^{-1} are assigned to bending vibrations of methylene groups. Whereas, the band at 705 cm^{-1} relates to the C–S stretching vibrations.[32]

Except the calcined SBA-15, other samples show distinct C–H vibrations at 2934 cm^{-1}, corresponding to C–H bond in the modified samples (Figure 2. b, c, d). Furthermore, SBA-15 modified samples (Figure 2.b, c, d) exhibit strong and broad absorption band at 3435 cm^{-1}, due to N–H stretching vibration which overlap with the –OH stretching frequency. All the modified SBA-15-SH, SBA-15-SH-TAT and SBA-15-SH-TAT-Pd(II) exhibit strong band at 1571 cm^{-1}, due to ring >C-N stretching vibration and additional peak at 1168 cm^{-1} (C–N) gets overlap with the symmetric stretching vibrations of the Si–O–Si bonds (1088 cm^{-1}).[33] The above mode of vibrations clearly indicate that 2, 4, 6-triallyloxy-1, 3, 5-triazine Pd(II) complex and organic modifiers were incorporated successfully over the surface modified SBA-15.

The diffuse reflectance spectra (200–800 nm) of calcined SBA-15 and SBA-15-TAT-Pd(II) show the characteristic absorption at 254 nm, corresponds to typical siliceous material (Figure 3.a).[34] SBA-15-TAT-Pd(II) shows characteristic absorption band at 260 nm corresponding to a metal-ligand charge transfer (MLCT). The shift towards higher energy values result from the metallation by Pd acetate. The presence of high coordinating ligand like 2, 4, 6-triallyloxy-1, 3, 5-triazine (TAT), the Pd(II) shifts the absorbance band towards the higher frequency region resulting in a slight deviation from theoretical values. Another strong absorbance at 380 nm *i.e.* in the visible region may be due to a change in π→π* and at 682 nm corresponds to n→π* transitions after Pd grafting over organo-modified SBA-15-TAT complex[32] (Figure 3.b). These results are in agreement with XPS results.

The organic moiety 2, 4, 6-triallyloxy-1, 3, 5-triazine anchored over the modified (–SH) surface of SBA-15 is further demonstrated by ^{13}C NMR techniques. ^{13}C Liquid NMR of 2, 4, 6-triallyloxy-1, 3, 5-triazine (TAT) and ^{13}C solid state NMR spectrum of SBA-15-TAT-Pd(II) are depicted in Figure 4. a, b. The peaks at 8, 20 and 34 ppm, present in SBA-15-TAT-Pd(II) catalyst are assigned to the carbon atoms (C1–C3) of the propyl chain in organic modifier (3-MPTMS), indicate the successful 3-Mercaptopropyl trimethoxysilane functionalization over SBA-15 (Figure 4.b). The presence of new resonance in the ^{13}C CP MAS NMR spectrum and also in ^{13}C Liquid NMR of 2, 4, 6-triallyloxy-1, 3, 5-triazine (TAT), at 72 ppm corresponds to carbon attached to the oxygen atom in the allylic chain of triazene ligand (Figure 4. a, b). Furthermore, peak present in both TAT and SBA-15-TAT-Pd(II) at 169 ppm corresponds to the carbon present in the ring of triazene ligand (TAT). In addition, low intensity extra peaks in the range of 103–130 ppm corresponds to the unmodified allylic group of triazene ligand (Figure 4, a, b), which might be due to the unreacted portion of the allylic group of 2, 4, 6-triallyloxy-1, 3, 5-triazine ligand. Since; the intensity of the un-reacted carbon peak is lower, it is confirmed that the maximum amount of anchoring of TAT over 3-MPTMS modified SBA-15. All the resonance peaks of ^{13}C NMR support the successful anchoring of 2, 4, 6-triallyloxy-1, 3, 5-triazine over the 3-MPTMS modified SBA-15 surface.

The degree of functionalization of surface silanol groups of SBA-15 with organic moiety can be monitored by ^{29}Si CP MAS NMR spectroscopy. ^{29}Si CP–MAS NMR spectra of calcined SBA-15 and SBA-15-TAT-Pd(II) are depicted in Figure 5. The spectrum shows broad resonance peaks from –90 to –120 ppm, indicative for a range of Si–O–Si bond and the bands are centered at –93 ppm, –102 ppm and –111 ppm assigned to Q^2 [germinal silanol, $(SiO)_2Si(OH)_2$], Q^3 [single silanol, $(SiO)_3Si(OH)$] and Q^4 [siloxane, $(SiO)_4Si$] sites of the silica framework, respectively (Fig. 5. a, b). The calcined SBA-15 shows the presence of broad resonance peaks from –98 to –126 ppm, indicative for a range of Si–O–Si bond, and it is noteworthy that the sample contains large amounts of Q^4 sites showing a high framework cross-linking. In general, the Q^3 sites are considered to be rich with isolated Si–OH groups, which may be free or hydrogen-bonded. Spectrum of SBA-15-TAT-Pd(II) show two peaks at –67 ppm and at –60 ppm which are assigned to T^3 [$SiR(OSi)_3$] and T^2 [$Si(OH)R(OSi)_2$], respectively. The presence of major T^3 peak indicate that the proper heterogenization of 3-mercaptopropyltrimethoxy silane over SBA-15.[35] ^{29}Si CP MAS NMR spectra provide direct evidence for the formation of a highly condensed siloxane network with organic group covalently bonded to the mesoporous silica.[36]

TEM images of calcined SBA-15 and SBA-15-TAT-Pd(II) provide structural evidence that the material is organized into ordered arrays of two-dimensional hexagonal mesopores (Figure 6.A.B). The significant difference of the TEM patterns was not observed between the two Figures 6.A, B. However, after the anchoring of TAT-Pd(II) complex inside the mesoporous channels of SBA-15, the image had shown distinct deep contrasting meso parallel channels with respect to the light shaded surface. This might be interpreted as due to the presence of the TAT-Pd(II) complex inside the mesopores of the SBA-15, but not on the surface. If the TAT-Pd(II) complex was anchored on the surface of the functionalized SBA-15, then the high-contrast dark meso parallel channels would have appeared along the boundary of the visualized SBA-15 and not inside the porous body as observed previously by *Shephard et al.*[37] From this results it is very clear that the Pd-complex was immobilized inside the pore channels of modified SBA-15. SEM image of the calcined SBA-15 and SBA-15-TAT-Pd(II) are shown in Figure 7 A, B, respectively. Calcined SBA-15 shows uniform arrays of small agglomerate particle meso channals arrangement and clear molecular-scale periodicity in the SEM images. Furthermore, SBA-15-TAT-Pd(II) demonstrates molecular-based materials; the particle morphology in the large molecular system does not change and becomes denser after TAT-Pd(II) complex anchoring over the mesoporous surface in comparison to the calcined SBA-15.

Thermal stability of all the synthesized materials were studied by thermo gravimetric analysis (TGA) under air atmosphere from ambient temperature to 1000 °C with a temperature increment of 10 °C/min. TGA and DTA of (a) As-synthesized SBA-15, (b) Calcined SBA-15, (c) SBA-15-SH and (d) SBA-15-TAT are shown in the Figure 8.A, B. TGA plots of calcined SBA-15 and modified SBA-15 samples show approximately 5 % weight loss below 120 °C caused due to the desorption of physiosorbed water molecules (Figure 8.A, a-d).[38-40] A loss of ~56 weight % was observed between 132 °C and 400 °C for the as-synthesized SBA-15 corresponds to the removal of trapped surfactant within closed pores (Figure 8.A, a). Whereas, nearly no weight loss in TGA was observed in the calcined SBA-15 between 132 °C and 400 °C indicates the complete removal of surfactant from SBA-15. Moreover a total weight loss of ~ 7 % was noticed for calcined SBA-15 and this may be due to removal of surface silanol groups at very high temperature (Figure 8, A, b). TGA result of SBA-15-SH samples shows weight loss in two steps. In the first step, weight loss was occurred between 70 °C and 150 °C corresponds to the loss of loosely bounded water and adsorbed moisture. In the second step, weight loss was observed in the region of 245 °C-385 °C in TGA analysis and a sharp exothermic peak visible in DTA analysis is attributed to decomposition of 3-MPTMS (Figure 8.A, B, c).

TGA result of SBA-15-SH material shows quantitatively 14.27 % weight loss, which is greater than calcined SBA-15; strongly supports successful anchoring of 3-MPTMS over SBA-15 (Figure 8.A, b, c). In the case of SBA-15-TAT samples, a total weight loss of ~35 % was noticed, is due to complete decomposition of organic moieties heterogenized over SBA-15, which is supported by the exothermic peak in the DTA spectrum of the same sample (Figure 8.B.d). All the TGA and DTA results clearly indicate that 2, 4, 6 -triallyloxy-1, 3, 5-triazine is well anchored over the modified surface of calcined SBA-15.

The nitrogen adsorption–desorption results of calcined SBA-15, SBA-15-TAT-Pd(II) and their corresponding pore size distribution curves are plotted in Figure 9. The surface area, average pore diameter and pore volume determined for the calcined SBA-15 and SBA-15-TAT-Pd(II) are summarized in the Table 1. All the samples show type IV adsorption isotherms, according to the IUPAC classification, indicating mesopores with completely reversible nature, uniformly sized, with a capillary condensation step at P/Po = 0.3–0.4. The total surface area, average pore diameter and pore volume observed for the calcined SBA-15 and SBA-15-TAT-Pd(II), were found to be 830 m^2/g, 65 Å, 1.13 cm^3/g and 285 m^2/g, 55 Å, 0.46 cm^3/g, respectively. The decrease in total mesoporous surface area (65 %), pore diameter (15 %) and pore volume (59 %) after 2, 4, 6 -triallyloxy-1, 3, 5-triazine Pd(II) complex immobilization over organo-modified SBA-15 is indicative of the grafting of TAT-Pd(II) complex over the mesoporous SBA-15 (Table 1).

It is clear from Table 1 that even though silylation procedures changed the textural properties of the mesoporous material, the decrease is more prominent after 2, 4, 6 -triallyloxy-1, 3, 5-triazine Pd(II) complex immobilization over SBA-15 since the bulkier organic moieties inside the pore channels occupy more area of the void space (Figure 9 inset a, b). The capillary condensation steps of SBA-15-TAT-Pd(II) get reduced to lower P/Po values compared to calcined SBA-15 (Figure 9.a, b). This shift towards slightly lower partial pressure shows a possible reduction in the pore size and a partial distortion in pore arrangement, consistent with the XRD results. It is also known that the inflection position in N$_2$ sorption isotherms depends on the diameter of the mesopores and the sharpness usually indicates the uniformity of the mesopores, due to capillary condensation of nitrogen molecule. These results directly supporting the previous results of proper heterogenization of metal complex inside the mesoporous channels of the SBA-15.

X-ray photoelectron spectroscopy (XPS) is the powerful tool to investigate the electronic properties of the species formed on the surface of the materials. XPS is highly sensitive to electronic environment, e.g. oxidation state and or multiplicity influences in the binding energy of the core electron of the metal. The synthesized material SBA-15-TAT-Pd(II) was characterized by X-ray photoelectron spectroscopy (XPS) to ascertain the oxidation state of Pd species. In Figure 10 the Pd binding energy of SBA-15-TAT-Pd(II) exhibits two strong peaks centered at 337.9 eV. and 344 eV., respectively, which are assigned to the Pd 3d$_{5/2}$ and Pd 3d$_{3/2}$, respectively. The observed peaks indicate that palladium is present in the Pd^{2+} oxidation state in the synthesized SBA-15-TAT-Pd(II). According to literature report pure Pd acetate metal salt binding energy for Pd 3d$_{5/2}$ and Pd 3d$_{3/2}$ orbital appears at 338.2 eV. and 345.3 eV., respectively.[41] In comparison to literature value, the synthesized SBA-15-TAT- Pd(II) show shift in binding energy of Pd towards lower value *viz* 337.9 eV. Pd 3d$_{5/2}$ and 344 eV. Pd 3d$_{3/2}$, respectively. The decrease of Pd binding energy in 2, 4, 6 -triallyloxy-1, 3, 5-triazine complex functionalized SBA-15 implies that there is a strong coordination interaction between Pd metal species and 2, 4, 6 -triallyloxy- 1, 3, 5-triazine ligand.[42] These results are in agreement with the UV-vis observations.

Catalyst SBA-15-TAT-Pd(II) screening for Hydrogenation Reactions

Hydrogenation is one of the most basic chemical transformations of organic substances. Olefin and nitro compounds hydrogenation is an industrially important reaction. The catalytic activity of SBA-15-TAT-Pd(II) was tested in the hydrogenation of a variety of unsaturated olefin and aromatic nitro compounds to their corresponding products. The catalytic performance of the heterogenized catalyst SBA-15-TAT-Pd(II) in olefin hydrogenation was initially studied with styrene as the substrate under mild reaction conditions (Pressure H_2 = 150 psi, T = 40 °C). The reactions were carried out in methanol solvent at room temperature and under 100 psi hydrogen pressure. Detailed observations of all the reactions are given in Table 2. It is evident from the Table 2 that the SBA-15-TAT-Pd(II) is quite active for the hydrogenation reaction under mild reaction conditions. In the case of styrene and α-methyl styrene, the hydrogenated products (ethylbenzene & cumene) were obtained within 15 min, 45 min with 2320, 2320 TON, respectively (Table 2, entries 1, 5). The reason for longer reaction time period for α-methyl styrene might be due to the steric hindrance produced by the methyl group next to the olefin group. In the absence of SBA-15-TAT-Pd(II) catalyst, negligible styrene conversion was observed (~7 %). It is noteworthy to mention that no ring hydrogenated products were observed with styrene, and α-methyl styrene.

Non-aromatic cyclic olefin group containing substrates cyclopentene, cyclohexene and cyclooctene gave hydrogenated products in 30 min, 60 min, 90 min with 2320, 2320, 1850 TON, respectively (Table 2, entries 7, 2, 3). The increase in reaction time for non-aromatic cyclic olefin containing substrates may be due to the increase in size of ring in term of carbon atoms. Whereas 1-hexene affords 100 % conversion to the corresponding hydrogenated product hexane in 15 min with 2320 TON. It is clear from the Table 2 that acyclic olefins afford higher rate of reaction in comparison to the cyclic olefin in presence of SBA-15-TAT-Pd(II); the reason might be that the olefin group faces steric hindrance in cyclic structure of aromatic or non-aromatic compounds. Furthermore, the SBA-15-TAT-Pd(II) catalyst affords 100 % conversion of the aromatic nitro (nitrobenzene) in 1 h with 2200 TON without the ring hydrogenation (Table 2, entry 4). The *trans*-stilbene, did not give any product under the specified time period. This is probably due to the relatively large steric hindrance (Table 2, entry 6) of the reactant molecule.

In contrast, commercial 10% Pd/C was used to hydrogenate styrene; it takes 60 min to complete the reaction, whereas the SBA-15-TAT-Pd(II) completed the reaction within 15 min under similar experimental conditions (Table 2, entry 9).

Heterogeneity and Recycling Studies of Catalyst SBA-15-TAT-Pd(II)

In order to understand whether the observed catalytic activity arises from truly heterogeneous catalyst systems, a series of leaching experiments was conducted. To test if metal is leached out from the solid catalyst during a reaction; the hot filtration test and recycling study of heterogeneous catalyst SBA-15-TAT-Pd(II) under the reaction conditions; 10 mmol of styrene, 150 psi of H_2 pressure, 0.025 g of catalyst SBA-15-TAT-Pd(II), 50 mL methanol, T = 40 °C was performed.

Hydrogenation reaction mixture was collected by filtration at temperature (40 °C) after a reaction time of 5 min which give 58 % conversions of styrene. The residual activity of the supernatant solution was studied. It was observed that after filtration of SBA-15-TAT-Pd(II) catalyst from the reaction mixture at the elevated reaction temperature (40 °C) (in order to avoid possible re-coordination or precipitation of soluble palladium upon cooling) hydrogenation reactions did not proceed further. Thus, results of the hot filtration test suggest that Pd was not being leached out from the solid catalyst during the reaction. These results confirm that the palladium catalyst remains on the support. This clearly demonstrate that the reaction ceased after the removal of SBA-15-TAT-Pd(II) catalyst from the reaction mixture.

Reusability is an important feature to be monitored for application of heterogenized single-site catalysts. Reusability of heterogeneous catalyst SBA-15-TAT-Pd(II) was performed under the reaction conditions; 10 mmol of styrene, 150 psi of H_2 pressure, 0.025 g of catalyst SBA-15-TAT-Pd(II), 50 mL methanol solvent, T = 40 °C. Hydrogenation reaction mixture was filtered using a sintered glass funnel, and the residue extensively washed with, 1, 2 dichloromethane (DCM) (2-5 mL) and further with methanol. The gas chromatography analysis of the filtrate shows no detectable amounts of reagents and products. The catalyst was dried under vacuum overnight before performing the reusability test. The catalyst could be reused directly without further purification and was reused up to five cycles (Figure 11). The amounts of Pd leaching into solution for the hydrogenation reactions were detected through ICP. The loss of Pd amount for the hydrogenation reaction was less than 1.0 weight percentage of total Pd content. Even though a small amount of Pd loss could be detected, catalyst still shows high reusability and stability for hydrogenation reactions. Nearly similar conversion was found even after five cycles by using SBA-15-TAT-Pd(II) catalyst in the hydrogenation reaction.

XPS analyses of fresh SBA-15-TAT-Pd(II) and spent SBA-15-TAT-Pd(II) catalyst (Five recycle) have been carried out to probe the change in the oxidation state of palladium in its coordination sphere (Figure S1, in the Supplementary Information). The XPS spectrum of the recycled catalyst clearly shows the presence of peaks at 337.5 eV and 342.6, corresponding to 3d5/2 and 3d3/2 respectively, of Pd(II) species the absence of peaks at 335.6 eV and 340.7 eV, corresponding to Pd(0) moiety. Even after repeated cycles of the hydrogenation reaction, catalyst SBA-15-TAT-Pd(II) shows the same Pd 3d peaks (Figure S1) (spent and fresh), suggesting that the oxidation state of the immobilized Pd did not change in repeated hydrogenation reactions.

Conclusions

In summary, highly stable and recyclable SBA-15-TAT-Pd(II) catalyst was synthesized by anchoring 2, 4, 6-triallyloxy-1, 3, 5-triazine complex over the surface of organo-functionalized SBA-15-SH and subsequent complexation with Pd acetate. Modified SBA-15 and SBA-15-TAT-Pd(II) were analyzed by elemental analysis, ICP–OES, XRD, N_2 sorption measurement isotherm, TGA & DTA, solid state ^{13}C & ^{29}Si NMR spectra FT-IR, XPS, DRS UV–Vis, SEM and TEM. Textural properties of synthesized catalyst and confirmation of 2, 4, 6-triallyloxy-1, 3, 5-triazine Pd(II) complex attached to

SBA-15 are revealed by XRD and N_2 sorption analyses. The (100), (110) and (200) reflections in SBA-15 show the structural stability. The thermal stability of synthesized SBA-15-TAT-Pd(II) was monitored by TGA–DTA. Solid state ^{13}C NMR spectra and FT-IR spectroscopy evidently support the organic moieties anchored over the surface of SBA-15 and inside the pore wall. Furthermore, solid state ^{29}Si NMR spectroscopy provides the information about degree of silylation. The electronic environment and oxidation state of Pd in SBA-15-TAT-Pd(II) were confirmed by XPS, DRS UV–vis techniques. Subsequently, the morphologies information of synthesized catalyst was monitored by SEM and TEM analysis. The catalytic activity of newly synthesized heterogeneous catalyst SBA-15-TAT-Pd(II) was screened in the hydrogenation reaction and found highly active in comparison to the commercial catalyst (10 wt. % Pd/C) within specific reaction time period under similar optimized reaction conditions. The present SBA-15-TAT-Pd(II) catalytic system tolerates a broad range of olefin compounds in hydrogenation reaction. The heterogenized solid catalyst SBA-15-TAT-Pd(II) can be recycled efficiently and reused several time (Five times) without major loss in activity.

Experimental

Synthesis of 2, 4, 6 -triallyloxy-1, 3, 5-triazine anchored SBA-15 and Pd metalation

In a typical synthesis, 1 g of organofunctionalized SBA-15, (3-Mercaptopropyl trimethoxysilane) was added to the solution containing 1.06 g solution of 2, 4, 6 -triallyloxy-1, 3, 5-triazine and 0.1 g of azobisisobutyronitrile (AIBN) (initiator) in 20 mL of DMF and refluxed at 100 °C for 24 h under nitrogen atmosphere. The solid was filtered and soxhlet-extracted with dichloromethane for 24 h. The resultant material was dried in vacuum for 2 h. Pd acetate (0.157 mmol) in 20 mL distilled DMSO (Dimethyl sulfoxide) was added in triazene modified SBA-15-SH solution and stirred at 85 °C for 12 h [Scheme 1(B, C)]. The resultant material was washed with THF and soxhlet extracted with dichloromethane (DCM) to remove the unanchored metal complex from the SBA-15 surface.[43]

Acknowledgements

Notes and references

A. P. Singh

Catalysis Division

CSIR-National Chemical Laboratory

Pune 411008, India

Fax: +91 20 2590 2633; Tel: +91 20 2590 2497;

E-mail: ap.singh@ncl.res.in

1　O. Schmidt, *Chem. Re*v. 1933, **12,** 363.

2　R. A. W. Johnstone, A. H. Wilby, I. D. Entwistle, *Chem. Rev.* 1985, **85,** 129.

3　C. M. Crudden, D. Allen, M. D. Mikoluk, J. Sun, *Chem. Commun.* 2001, 1154.

4　B. Chen, U. Dingerdissen, J. G. E. Krauter, H. G. J. Lansink Rotgerink, K. M¨obus, D. J. Ostgard, P. Panster, T. H. Riermeier, S. Seebald, T. Tacke, H. Trauthwein, *Appl. Catal: A*, 2005, **280,** 17.

5　K. Nomura, *J. Mol. Catal. A: Chem.*, 1998, **130,** 1.

6　H. U. Blaser, C. Malan, B. Pugin, F. Spindler, H. Steiner, M. Studer, *Adv. Synth. Catal.* 2003, **345,** 103.

7　a) R. M. Magdalene, E. G. Leelamani, N. M. N. Gowda, *J. Mol. Catal. A: Chem.* 2004, **223,** 17.; b) A. Molnar, G. V. Smith, M. Bartok', *J. Catal.*, 1986, **101,** 540.; c) A. Molnar, G. V. Smith, M. Bartok', *J. Catal.*, 1986, **101,** 67.; d) A. Mastalir, Z. Király, G. Szöllösi, M. Bartók, *Applied Catal A: Chem* 2001, **213**, 133.; e) Handbook of Heterogeneous Catalytic Hydrogenation for Organic Synthesis, Shigeo Nishimura, Publisher Wiley, 2001, ISBN 0471396982, 7980471396987.

8　a) *The Handbook of Homogeneous Hydrogenation* (Eds.: J. G. de Vries, C. J. Elsevier), Wiley-VCH, Weinheim, **2007.**; b) P. W. N. M: van Leeuwen, *Homogeneous Catalysis— Understanding the Art, Kluwer Academic Publ.,* Dordrecht, **2004,** chap. 4.; c) S. Bhaduri, D. Mukesh, Hydrogenation of Alkenes, Wiley, NY, 2000; d) A Bçrner, J. Holz, *Homogeneous Hydrogenations, in Transition Metals for Organic Synthesis,* Vol. 2, 2nd ed. (Eds.: M. Beller, C. Bolm), Wiley-VCH, Weinheim, 2004.

9　*a*) M. M. Dell'Anna, M. Gagliardi, P. Mastrorilli, G. P. Suranna, C. F. Nobile, *J. Mol. Catal. A: Chem.* 2000, **158,** 515.; b) Y. Zheng, K. Ma, H. Wang, X. Sun, J. Jiang, C. Wang, R. Li, J. Ma, *Catal. Lett.* 2008, **124,** 268.; *c*) A. J. Amali, R. K. Rana, *Chem. Commun.*, 2008, 4165.

10　*a*) N. Erathodiyil, S. Ooi, A. M. Seayad, Y. Han, S. S. Lee, J. Y. Ying, *Chem.–Eur. J.*, 2008, **14,** 3118.; b) K. C. Nicolaou, A. L. Nold, R. R. Milburn, C. S. Schindler, K. P. Cole, J. Yamaguchi, *J. Am. Chem. Soc.*, 2007, **129,** 1760.; c) F. Zhao, K. Murakami, M. Shirai, M. Arai, *J. Catal.*, 2000, **194,** 479.

11　*a*) A. Biffis, M. Zecca, M. Basato, *J. Mol. Catal. A: Chem.*, **2001,** 173, 249.; b) L. Yin and J. Liebscher, *Chem. Rev.*, 2007, **107,** 133.

12　D. H. Lee, J. Y. Jung, M. J. Jin. *Chem. Commun.* 2010, **46,** 9046.

13　J. Yang, L. Wang. *Dalton Trans.* 2012, **41,** 12031.

14　I. Blaszczyk, A. M. Trzeciak. *Tetrahedron.* 2010, **66,** 9502.

15　C. T. Kresge, M. E. Leonowicz, W. J. Roth, J. C. Vartuli, J. S. Beck. *Nature.* 1992, **359,** 710.

16　Y. Jackie, Ying, P. Christian, S. Mehnert, S. Michael, Wong. *Angew. Chem. Int. Ed.* 1999, **38,** 56.

17　G. J. de A. A. Soler-Illia, C. Sanchez, B. Lebeau, J. Patarin. *Chem. Rev.* 2002, **102,** 4093.

18　A. Walcarius, L. Mercier. *J. Mater. Chem.* 2010, **20,** 4478.

19　L. Nicole, C. Boissiere, D. Grosso, P. Hesemann, J. Moreau, C. M. Sanchez. *Chem. Commun.* 2004, 2312.

20　A. Corma. *Chem. Rev.* 1997, **97,** 2373.

21 Quach, V. Escax, L. Nicole, P. Goldner, O. Guillot-Noel, P. Aschehoug, P. Hesemann, J. Moreau, D. Gourier, C. Sanchez. *J. Mater. Chem.* 2007, **17,** 2552.

22 Z. Luan, M. Hartmann, D. Zhao, W. Zhou, L. Kevan. *Chem. Mater.* 1999, **11,** 1621.

23 A. Quach, V. Escax, L. Nicole, P. Goldner, O. Guillot-Noel, P. Aschehoug, P. Hesemann, J. Moreau, D. Gourier, C. Sanchez. *J. Mater. Chem.* 2007, **17,** 2552.

24 J. S. Beck, J. C. Vartuli, W. J. Roth, M. E. Leonowicz, C. T. Kresge, K. D. Schmitt, C. T-W. Chu, D. H. Olson, E. W. Sheppard, S. B. Mc Cullen, J. B. Higgins, J. L. Schlenker. *J. Am. Chem. Soc.* 1992, **114,** 10834.

25 D. Zhao, J. Feng, Q. Huo, N. Melosh, G. H. Fredrickson, B. F. Chmelka, G. D. Stucky. *Science.* 1998**, 279,** 548.

26 S. Sisodiya, A. Lazar, S. Shylesh, L. Wang, W. R. Thiel, A. P. Singh, *Catal. Comm.* 2012, **25,** 22.

27 P. Sharma, A. P. Singh, *Cat. Today.* 2012, **198,** 184. H. Wang, K. Schaefer, A. Pich, M. Moeller, *Chem. Mater.* 2011, **23,** 4748.

28 H. Wang, K. Schaefer, A. Pich, M. Moeller, *Chem. Mater.* 2011, **23,** 4748.

29 J. Galo, A. A. de, C. Soler-Illia, B. Sanchez, J. Lebeau, Patarin, *Chem. Rev.* 2002**, 102,** 4093.

30 T. W. Dijkstra, R. Duchateau, R. A. van Santen, A. Meetsma, G. P. A. Yap, J. *Am. Chem.* Soc. 2002, **124,** 9856.

31 N. H. Jentys, H. Pham, Vinek, J. *Chem. Soc. Faraday Trans.* 1996, **92,** 3287.

32 a) S. Srinivas, P. Ratnasamy. *Micro. Meso. Mat.* 2007, **105,** 170.; b) A. O. Adeloye, P. A. Ajibade. *Molecules* 2011, **16,** 4615.; c) B. Vlckov, V. Baumrukb, J. Mosinger *Journal of Molecular Structure,* 1992, **265,** 9.; d) A. Modak, J. Mondal, M. Sasidharan, A. Bhaumik. *Green Chem.* 2011, **13,** 1317.

33 A. Modak, J. Mondal, M. Sasidharan, A. Bhaumik, *Green Chem.* 2011, **13,** 1317.

34 T. Soundiressane, S. Selvakumar, S. Menage, O. Hamelin, M. Fontecave, A. P. Singh, *J. of Mol. Catal. A: Chem.* 2007, **270,** 132.

35 H. Yoshitake, T. Yokoi, T. Tatsumi, *Chem. Mater.* 2002, **14,** 4603.

36 P. Sharma, A. P. Singh. *Catal. Sci. Tech.* 2014**, 4,** 2978.

37 D. S. Shephard, W. Zhou, T. Maschmeyer, J. M. Matters, C. L. Roper, S. Parsons, B. F. G. Johnson, M. J. Duer, *Angew Chem. Int. Ed.* 37, 1998, **37,** 2719.

38 D. S. Shephard, W. Zhou, T. Maschmeyer, J. M. Matters, C. L. Roper, S. Parsons, B. F. G. Johnson, M. J. Duer, *Angew Chem. Int. Ed.* 37, 1998, **37,** 2719.

39 S. Shylesh, A. P. Singh, *J. Catal.* 2004, **228,** 333.

40 S. C. Laha, P. Mukherjee, S. R. Sainkar, R. Kumar, *J. Catal.* 2002, **207,** 213.

41 H. Yang, Y. Wang, Y. Qin, Y. Chong, Q. Yang, G. Li, Li, Zhang, W. Li, *Green Chem.* 2011, **13,** 1352.

42 R. Venkatesan, M. H. G. Prechtl, J. D. Scholten, R. P. Pezzi, G. Machado, J. Dupont. *J. Mater. Chem.* 2011, **21,** 3030.

43 Baleizao, B. Gigante, H. Garcia, A. Corma. *J. Cat.* 2003, **215,** 199.
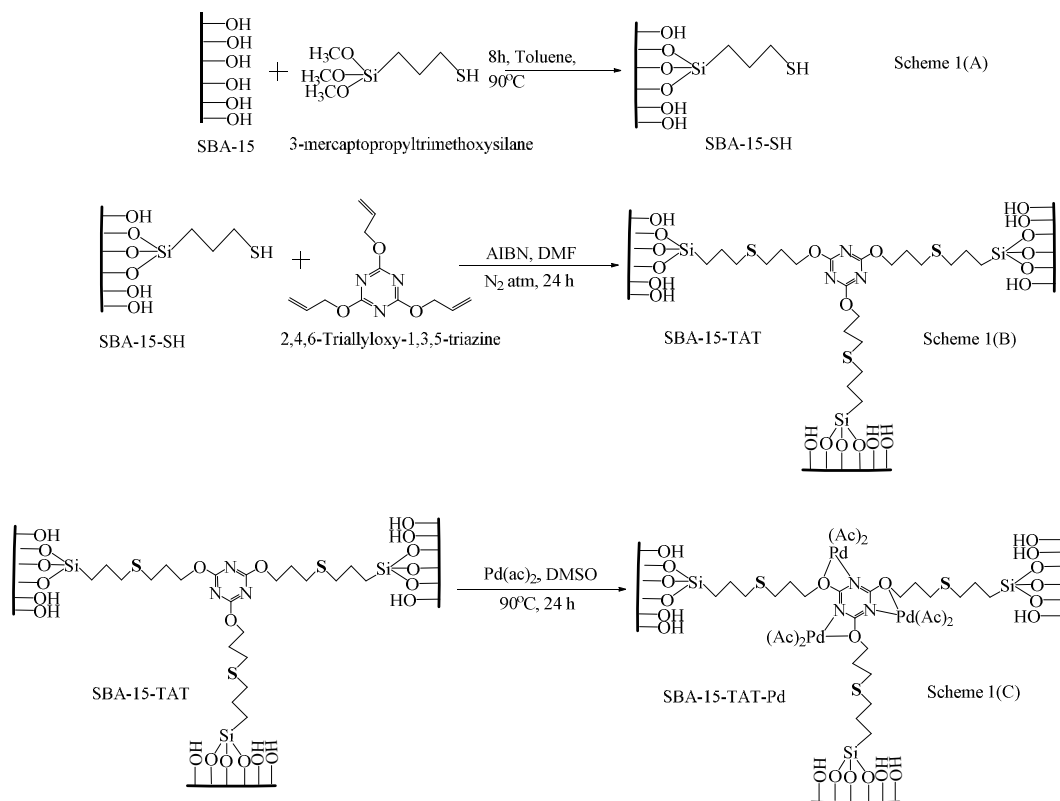
Scheme 1. Schematic diagram of heterogeneous SBA-15-TAT-Pd(II) synthesis. Surface Modification via 3-MPTMS (3-mercaptopropyl trimethoxysilane) of SBA-15, Scheme 1(B). Anchoring of 2, 4, 6-triallyloxy-1, 3, 5-triazine (TAT) complex over modified surface of SBA-15, Scheme 1(C). Metalation by Pd acetate.
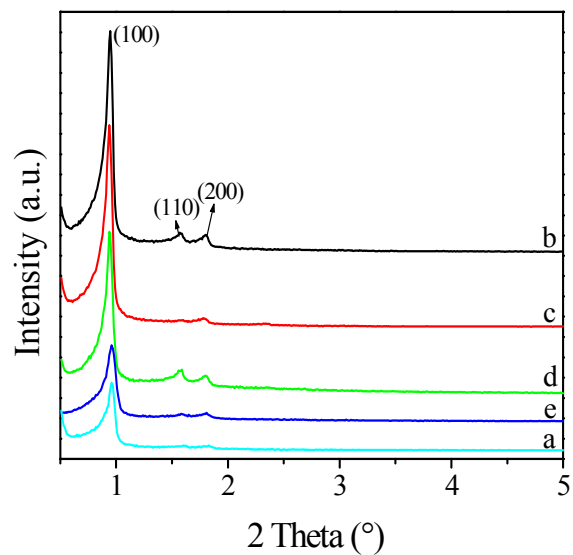
Fig.1. XRD pattern of (a) As-synthesized SBA-15, (b) Calcined SBA-15, (c) SBA-15-SH, (d) SBA-15-TAT, (e) SBA-15-TAT-Pd(II).
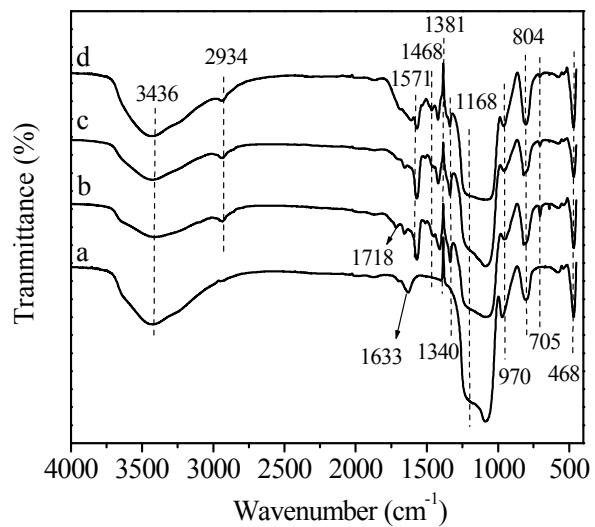
Figure 2. FT-IR spectrum of (a) Calcined SBA-15, (b) SBA-15-SH, (c) SBA-15 TAT and (d) SBA-15-TAT-Pd(II).
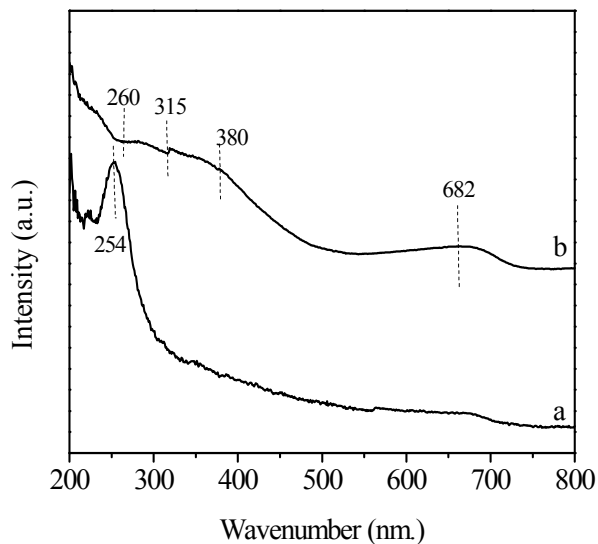
Figure 3. UV-vis spectra of (a) Calcined SBA-15 and (b) SBA-15-TAT–Pd(II).
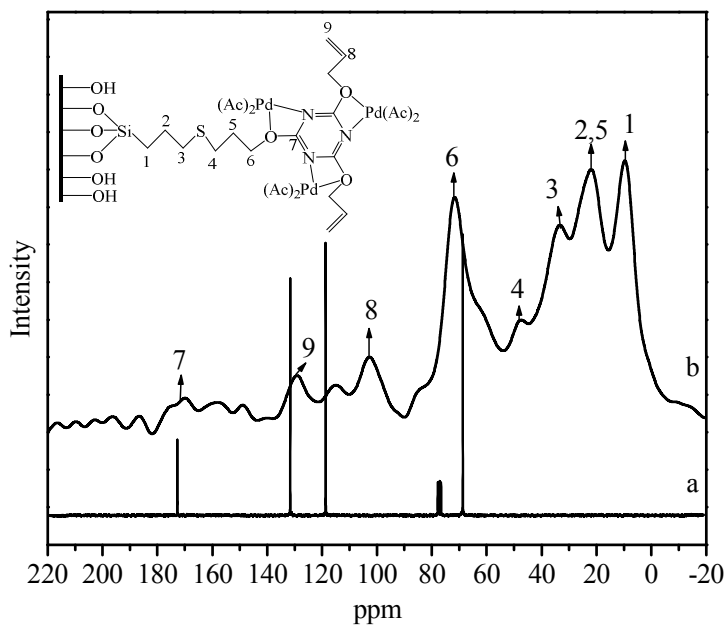
Figure 4. Liquid ^{13}C NMR of (a) 2, 4, 6-triallyloxy-1, 3, 5-triazine (TAT) and (b) Solid state ^{13}C CP MAS NMR of SBA-15-TAT-Pd(II).
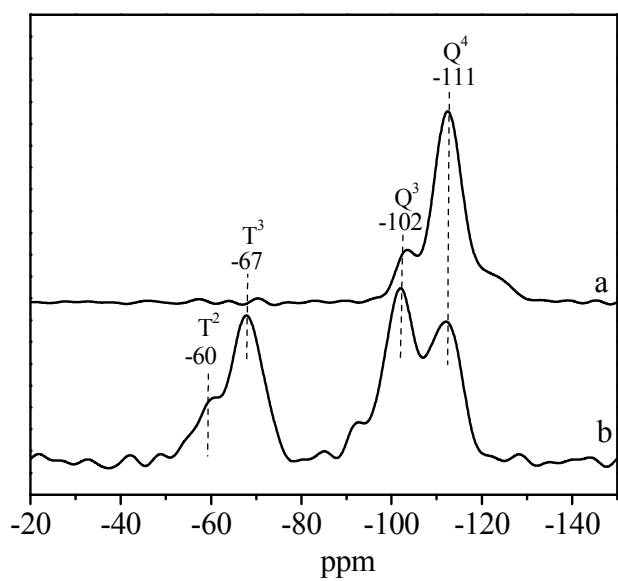
Figure 5. Solid state ^{29}Si CP MAS NMR spectrum of (a) Calcined SBA-15 and (b) SBA-15-TAT-Pd(II).
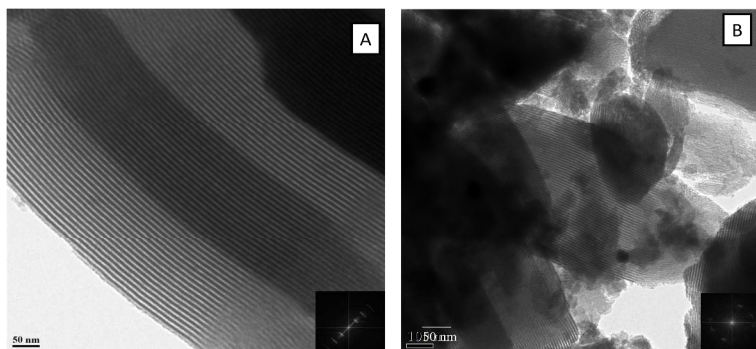
Figure 6. TEM Images (A) Calcined SBA-15 and (B) SBA-15-TAT-Pd(II).
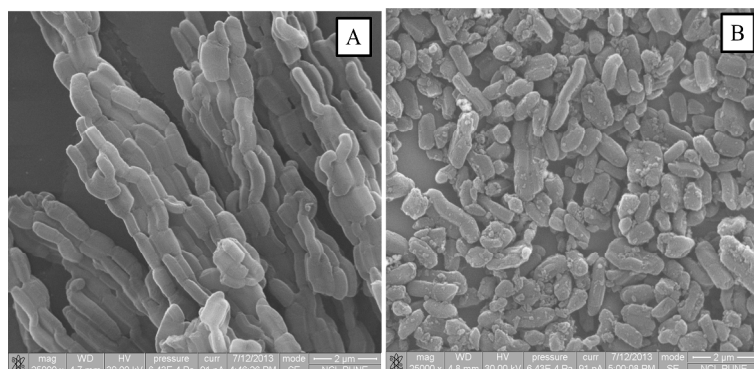
Figure 7. SEM images of (A) Calcined SBA-15 and (B) SBA 15-TAT-Pd(II).
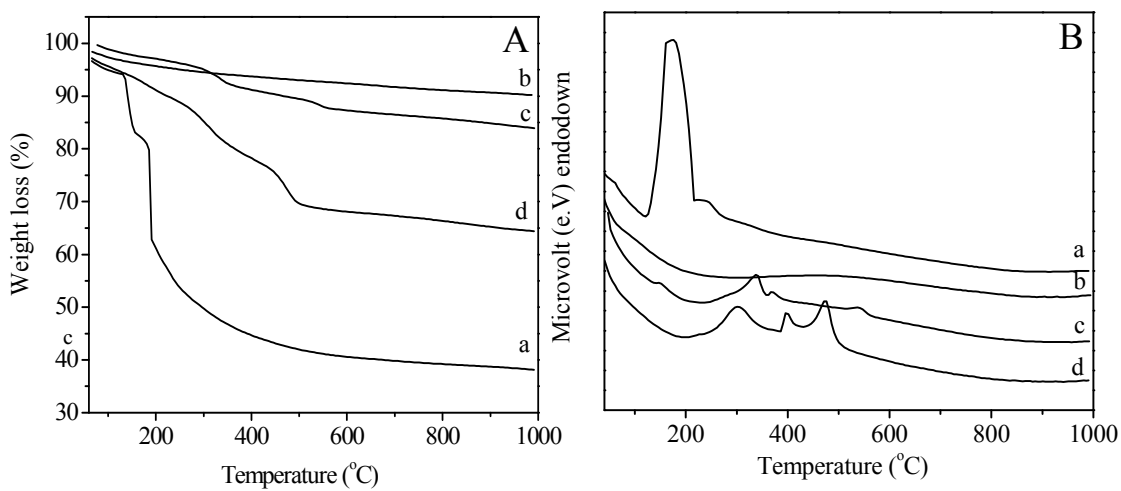
Figure 8. (A) TGA, (B) DTA of (a) As-synthesized SBA-15, (b) Calcined SBA-15, (c) SBA-15-SH and (d) SBA-15-TAT.
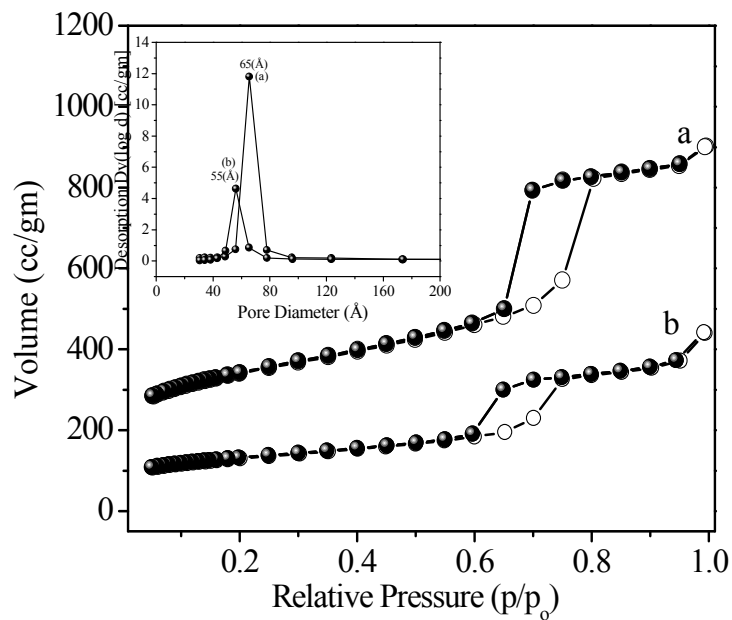
Figure 9. Nitrogen adsorption-desorption isotherm and inset (BJH) pore size distribution of (a) calcined SBA-15 and (b) SBA-15-TAT-Pd(II).
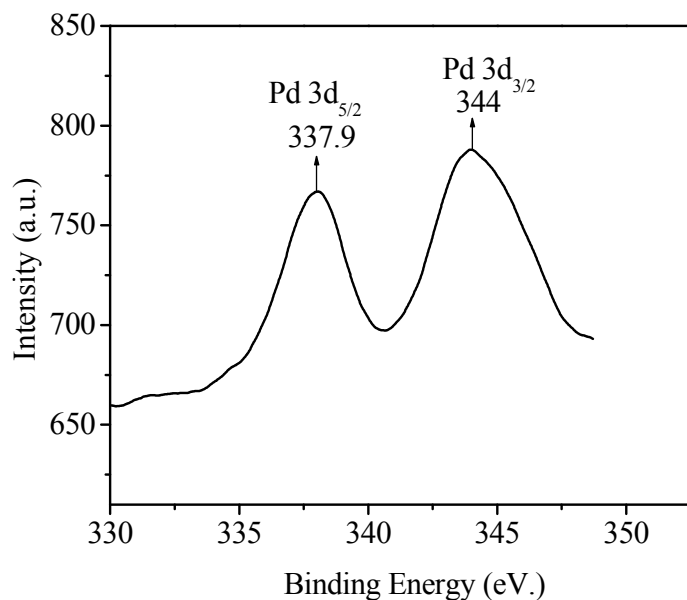
Figure 10. XPS spectra of SBA-15-TAT-Pd(II).

Table 1.

Textural properties of mesoporous calcined SBA-15 & SBA 15-TAT-Pd(II).

S.No.	Sample	N[a] (wt. %)	Loading of Pd (wt. %)[b]		S.A (m^2/g)	D$_P$ (Å)	Vp (cm^3/g)
			Input	Output			
1.	Calcined SBA-15				830	65	1.13
2.	SBA-15-TAT-Pd(II)	1.85	4	2.2	285	55	0.46

[a] Calculated based on elemental (Nitrogen) analysis value.

[b] Input is based on the amount of Pd during synthesis reaction; output is based on the ICP-OES analysis.

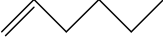S.A : BET scurface area (D$_P$) : Average pore diameter, (Vp) : Pore volume.
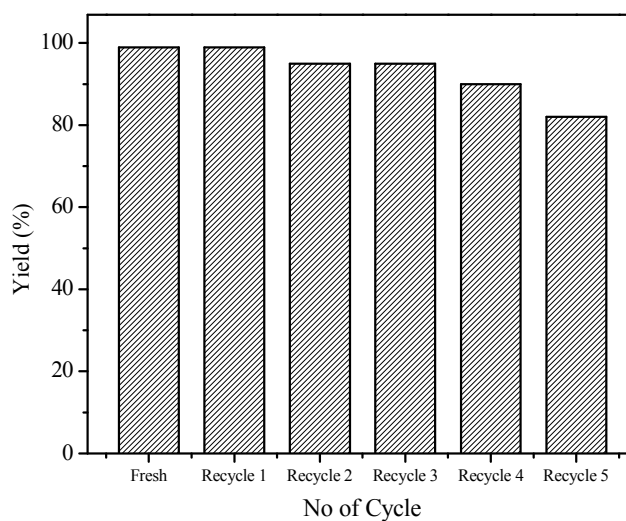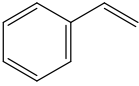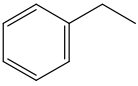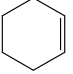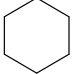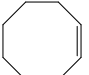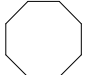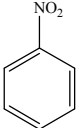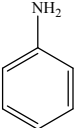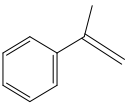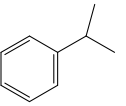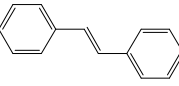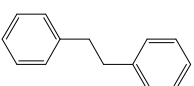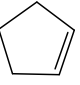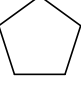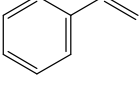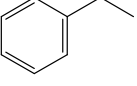

Figure 11. Recycling study of heterogeneous catalyst SBA-15-TAT-Pd(II).

Reaction Conditions: 10 mmol of styrene, 150 psi of H$_2$ pressure, 0.025 g of catalyst SBA-15-TAT-Pd(II), 50 mL methanol, T = 40 °C.

Table 2. SBA-15-TAT-Pd(II) catalyst for Hydrogenation Reaction.

S. No.	Reactant	Product	Time (min.)	Yield (%)	TON
1.			15	100	2320
2.			60	100	2320
3.			90	80	1850
4.			60	95	2200
5.			45	100	2320
6.			480	---	---
7.			30	96	2230
8.			15	100	2320
9.#			60	100	-----

Reaction conditions: of substrate (10 mmol), SBA-15-TAT-Pd(II) catalyst (0.025 g), H_2 Pressure = 150 psi, Reaction Temperature = 40 °C, solvent = 50 mL methanol.
Reaction carried out in presence of 10 wt. % Pd/C.